Electronic Supplementary Material (ESI) for Journal of Materials Chemistry A.

Supplementary Information

Structure-Property Relationship of Metal-Organic Frameworks for Alcohol Adsorption based Heat Pumps by High-throughput Computational Screening

Wei Li, Xiaoxiao Xia , Meng Cao and Song Li *

State Key Laboratory of Coal Combustion, School of Energy and Power Engineering, Huazhong University of Science and Technology, Wuhan, China, 430074.

Table of Contents

S1. Computation details of COP_C based on GCMC simulations

Figure S1. Isothermal diagram of adsorption-driven heat pump cycle

The coefficient of performance (COP) of AHPs is defined as the ratio of the output energy and input energy. According to the isosteric diagram of AHP cycle as shown in Figure 1, COP_C for cooling and COP_H for heating can be defined by the following equations, respectively.

$$COP_C = \frac{Q_{ev}}{Q_{regen}} \quad \text{(Eq. S1)}$$

$$COP_H = \frac{-\left(Q_{con} + Q_{ads}\right)}{Q_{regen}} \quad \text{(Eq. S2)}$$

Here, Q_{con} is the energy released during condensation and Q_{ads} is the energy released during the adsorption stage. Both Q_{con} and Q_{ads} are negative values. Q_{ev} is the energy taken up in the evaporator. Q_{reg} is the energy required for regeneration of adsorbent, which can be obtained according to Eq. S3.

$$Q_{regen} = Q_{I\text{-}II} + Q_{II\text{-}III} = \int_{T_{con}}^{T_2} C_p^{effective}(T)dT + \int_{T_{con}}^{T_2} \rho_{liq}^{wf} W_{\max} C_p^{wf}(T)dT + \int_{T_2}^{T_{des}} C_p^{effective}(T)dT + \int_{T_2}^{T_{des}} \rho_{liq}^{wf} \frac{W_{\max} + W_{\min}}{2} C_p^{wf}(T)dT - Q_{sorption} \quad \text{(Eq. S3)}$$

$$Q_{sorption} = \frac{1}{M_w} \int_{W_{\min}}^{W_{\max}} \rho_{liq}^{wf} \Delta_{ads} H(W)dW \quad \text{(Eq. S4)}$$

Here, $\int_{T_{con}}^{T_2} C_p^{effective}(T)dT$ is the energy required for the adsorbent bed temperature to change from T_{con} to T_2; $\int_{T_{con}}^{T_2} \rho_{liq}^{wf} W_{\max} C_p^{wf}(T)dT$ is the energy required for the working fluids temperature to change from T_{con} to T_2; $\int_{T_2}^{T_{des}} C_p^{effective}(T)dT$ is the energy required for adsorbent bed temperature change from T_2 to T_{des}; $\int_{T_2}^{T_{des}} \rho_{liq}^{wf} \frac{W_{\max} + W_{\min}}{2} C_p^{wf}(T)dT$ is the energy required for the working fluid temperature to change from T_2 to T_{des}; $Q_{sorption}$ is the energy required for working fluid desorption in the AHP system.

Herein, the $C_p^{effective}$ is the heat capacity of adsorbents (i.e. C_p^{ads}), and C_p^{wf} is the working capacity of working fluid, both of which are assumed to be constants that does not change with the temperature (C_p^{ads} =1 kJ/(kg•K) for MOFs and C_p^{wf} = 2.2 kJ/(kg•K) for ethanol).[1] In addition, it is known that both ρ_{liq}^{wf} does not vary obviously with temperature either, therefore the term $\int_{T_{con}}^{T_2} \rho_{liq}^{wf} W_{\max} C_p^{wf}(T)dT + \int_{T_2}^{T_{des}} \rho_{liq}^{wf} \frac{W_{\max} + W_{\min}}{2} C_p^{wf}(T)dT$ was neglected. Eventually, the energy required for desorption and adsorbent temperature change contribute most to the regeneration energy as shown below.

$$Q_{regen} \approx \int_P^{MOFs} (T_{des} - T_{con}) - \frac{1}{M_w} \rho_{liq}^{wf} \langle \Delta_{ads} H \rangle \Delta W \quad \text{(Eq. S5)}$$

Here, the density of ethanol ρ_{liq}^{wf} was obtained by :

$$\ln \rho = \alpha_0 + \alpha_1 T + \alpha_2 T^2 + \alpha_3 T^3 + \alpha_4 T^4 + \alpha_5 T^5 \quad \text{(Eq. S6)}$$

Table S1. Parameters for ethanol density calculation in Eq.S6

α_0	α_1	α_2	α_3	α_4	α_5
-1.08×10^{-1}	-7.72×10^{-3}	1.59×10^{-4}	-1.61×10^{-6}	7.19×10^{-9}	-1.21×10^{-11}

The loading averaged enthalpy of adsorption was estimated by the following equation

$$\langle \Delta_{ads} H \rangle = \frac{\Delta_{ads} H_{\max} + \Delta_{ads} H_{\min}}{2} \quad \text{(Eq. S7)}$$

As the temperature increases from 303 K to 353 K, ethanol density decreases from 0.80×10^3 to 0.757×10^3 kg/m^3. The unit of ΔW herein was converted to g/g.

In an idealized AHP cycle, $Q_{ads} = -Q_{regen}$

Q_{ev} and Q_{con} can be obtained by the following equation:

$$Q_{ev} = -\frac{\Delta_{vap} H(T_{ev}) \rho_{liq}^{wf} m_{sorbent} \Delta W}{M_w} \quad \text{(Eq. 8)}$$

$$Q_{con} = \frac{\Delta_{vap} H(T_{con}) \rho_{liq}^{wf} m_{sorbent} \Delta W}{M_w} \quad \text{(Eq. S9)}$$

The ethanol vaporization enthalpy was also computed by:

$$\Delta_{vap} H = A \exp(-\alpha T_r)\left(1 - T_r\right)^{\beta} \quad \text{(Eq. S10)}$$

$$T_r = \frac{T}{T_c} \quad \text{(Eq. S11)}$$

Table S2. Parameters used for ethanol vaporization enthalpy calculation

Temperature (K)	A (kJ/mol)	α	β	T_c (K)
298-469	50.43	-0.4475	0.4989	513.9

T_c, critical temperature

$$COP_c = \frac{Q_{ev}}{Q_{regen}} = \frac{\dfrac{\Delta_{vap}H(T_{ev})\rho_{liq}^{wf} m_{sorbent}\Delta W}{M_w}}{-C_p^{sorbent}(T_{des}-T_{con}) + \dfrac{1}{M_w}\rho_{liq}^{wf}\langle\Delta_{ads}H\rangle\Delta W} \quad \text{(Eq. S 12)}$$

$$COP_H = \frac{-(Q_{con}+Q_{ads})}{Q_{regen}} = 1 + \frac{\dfrac{\Delta_{vap}H(T_{con})\rho_{liq}^{wf} m_{sorbent}\Delta W}{M_w}}{-C_p^{sorbent}(T_{des}-T_{con}) + \dfrac{1}{M_w}\rho_{liq}^{wf}\langle\Delta_{ads}H\rangle\Delta W} \quad \text{(Eq. S 13)}$$

The working conditions for adsorption cooling in this work are shown in Table S3.

Table S3. The operation temperatures in this work

	T_{ads}	T_{des}	T_{ev}	T_{con}
T (K)	303	353	283	303

The evaporation and condensation pressures were fixed at P_{ev} = 3000 Pa (i.e. P/P_o = 0.29 at 303 K) and P_{con} = 10400 Pa (i.e. P/P_o= 1.0 at 303 K), respectively.

Table S4. TraPPE force field parameters of ethanol

adsorbate	interaction site	σ (Å)	ε/k_B (K)	q (e)
ethanol	CH_3	3.75	98.0	0
	CH_2	3.95	46.0	0.265
	O	3.02	93.0	-0.7
	H	0	0	0.435

S2. Structure-property relationship of CoRE MOFs

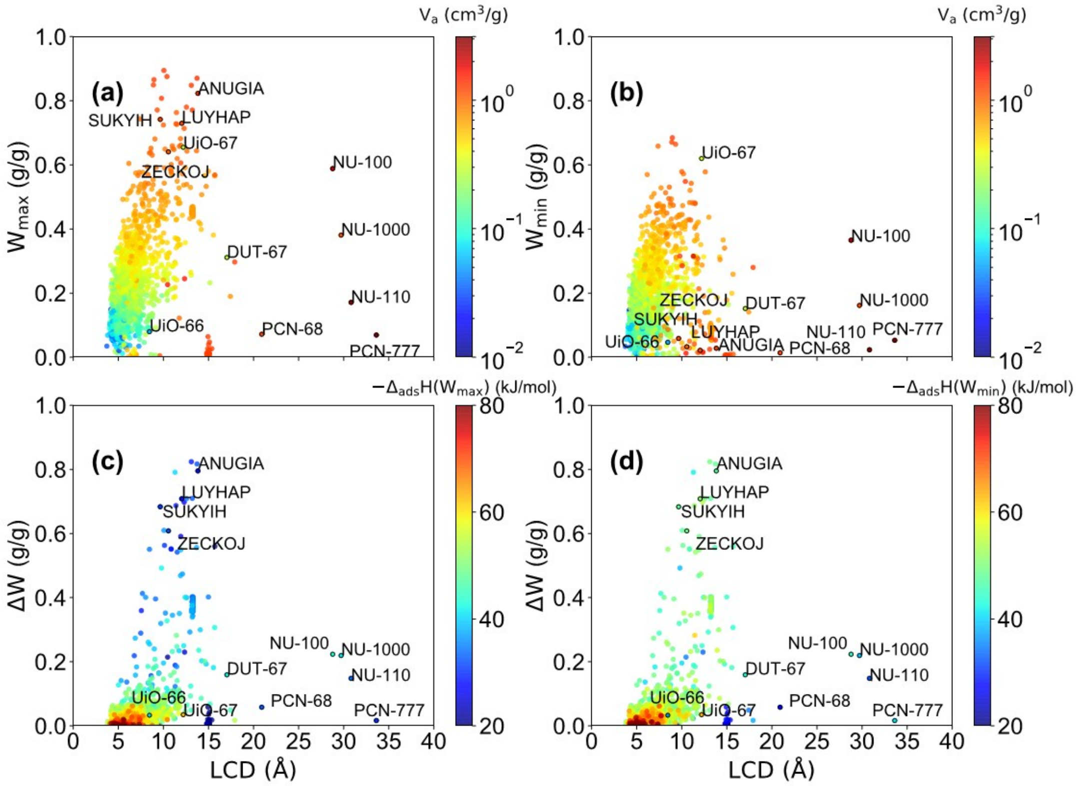

Figure S2. The predicted maximum (W_{max}) and minimum (W_{min}) adsorption capacity of 1527 CoRE MOFs as a function of largest cavity diameter (LCD) and accessible pore volume (a and b); the ethanol working capacity (ΔW) of 1527 CoRE MOFs as a function of LCD and the enthalpy of adsorption at maximum and minimum adsorption capacity (c and d). The working capacity was obtained from T_2 = 325 K and T_{des} = 353 K, respectively at fixed pressure (P= 10400 Pa).

Figure S3. Structure-property relationship of CoRE MOFs. (a) The relationship between COP_C, working capacity (ΔW) and the structural properties of MOFs (a) largest cavity diameter (LCD), (b) accessible surface area (ASA) and (c) accessible pore volume (V_a). (d), (e) and (f) show the correlation between COP_C, the load averaged enthalpy of adsorption (<Δ_{ads}H>) and the structural properties of (d) largest cavity diameter (LCD), (e) accessible surface area (ASA) and (f) accessible pore volume (V_a).The COP_C was obtained at fixed operational temperatures, in which T_{ads} = T_{con} = 303 K, T_{ev} = 283 K and T_{des} = 353 K.

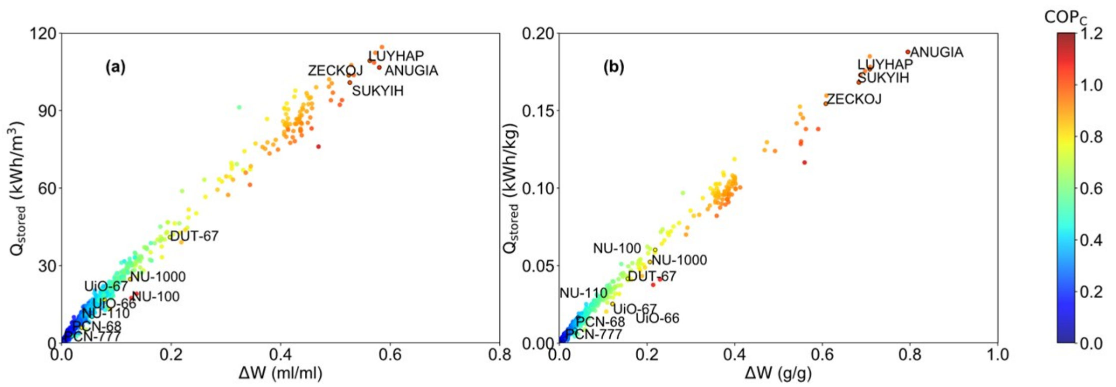

Figure S4. The correlation between the stored thermal energy (Q_{stored}) and working capacity (ΔW) of CoRE MOFs, colored by COP_C. Q_{stored} was obtained at fixed operational temperatures, in which $T_{ads} = T_{con} = 303$ K, $T_{ev} = 283$ K and $T_{des} = 353$ K.

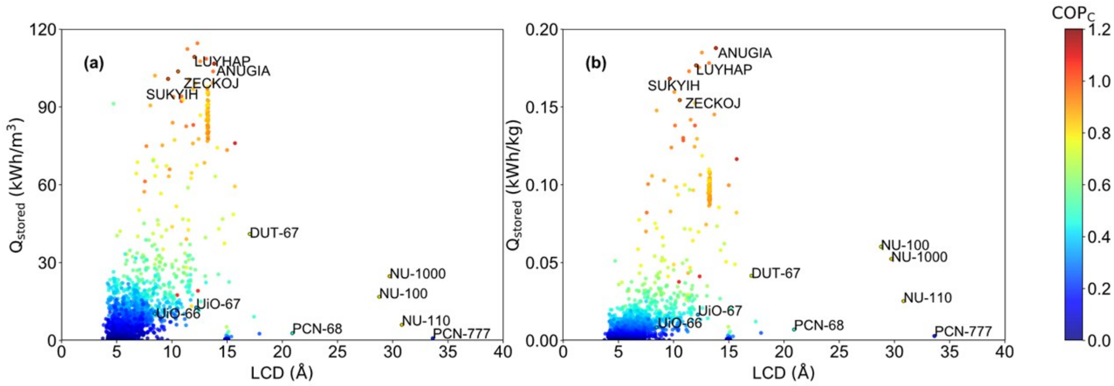

Figure S5. The structure-property relationship between the (a) amount of storable energy (Q_{stored}) per unit volume and (b) per unit mass and LCD of CoRE MOFs, respectively. Q_{stored} is identical to $Q_{sorption}$ as calculated according to Eq. S4.

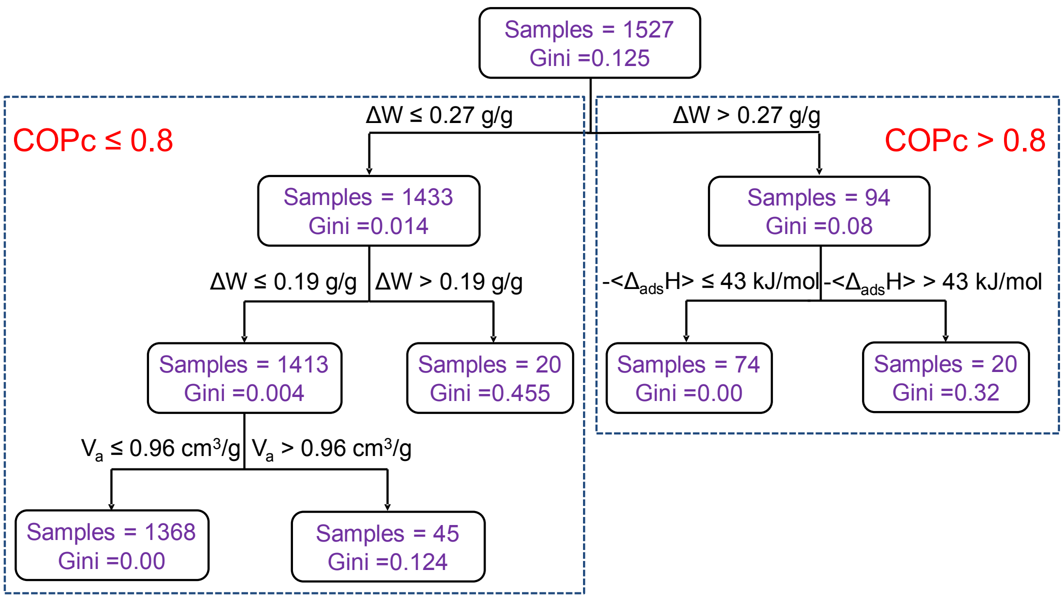

Figure S6. Decision tree analysis of 1527 CoRE MOFs based on different split criteria. 1433 MOFs with $COP_C \leq 0.8$ exhibited $0 < \Delta W \leq 0.27$ g/g and 94 MOFs $COP_C > 0.8$ exhibited $0.27 < \Delta W \leq 0.82$ g/g. For 1433 MOFs with $COP_C \leq 0.8$, 1413 MOFs exhibited $0 < \Delta W \leq 0.19$ g/g and 20 MOFs exhibited $0.19 < \Delta W \leq 0.27$ g/g. Among the 1413 MOFs with $0 < \Delta W \leq 0.19$ g/g, 1368 MOFs exhibited accessible pore volumes of $0.02 < V_a \leq 0.96$ cm^3/g, and 45 MOFs exhibited $0.96 < V_a \leq 3.11$ cm^3/g. Among the 94 MOFs with $COP_C > 0.8$, 74 MOFs exhibited the averaged enthalpy of adsorption of $28.1 < -\langle\Delta_{ads}H\rangle \leq 43$ kJ/mol, and 20 MOFs exhibited $43 < -\langle\Delta_{ads}H\rangle \leq 45.8$ kJ/mol.

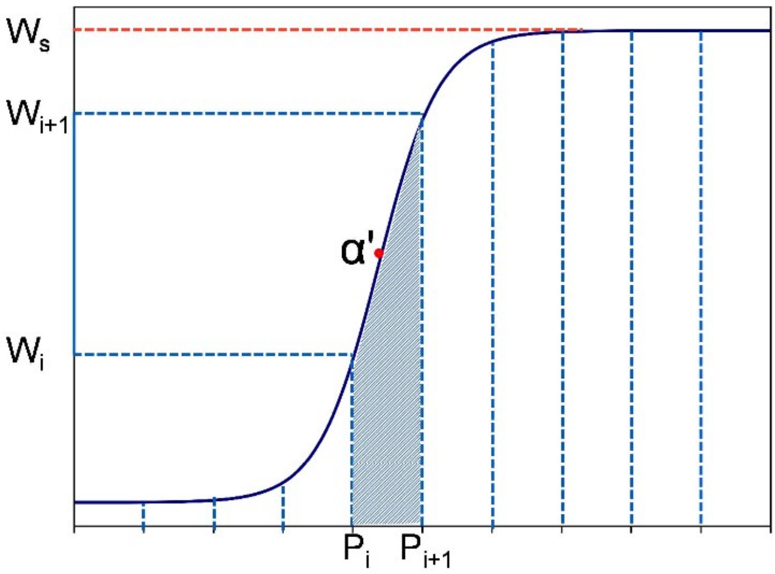

Figure S7. The definition of step position range according to the shape of ethanol adsorption isotherm of MOFs at 303 K. W_s is the saturated adsorption capacity. Ten pressure ranges (i = 0-9) were identified every P/P_0 = 0.1. When $(W_{i+1} - W_i)/ W_S \geq 0.5$, the step position $P_i < \alpha' \leq P_{i+1}$.

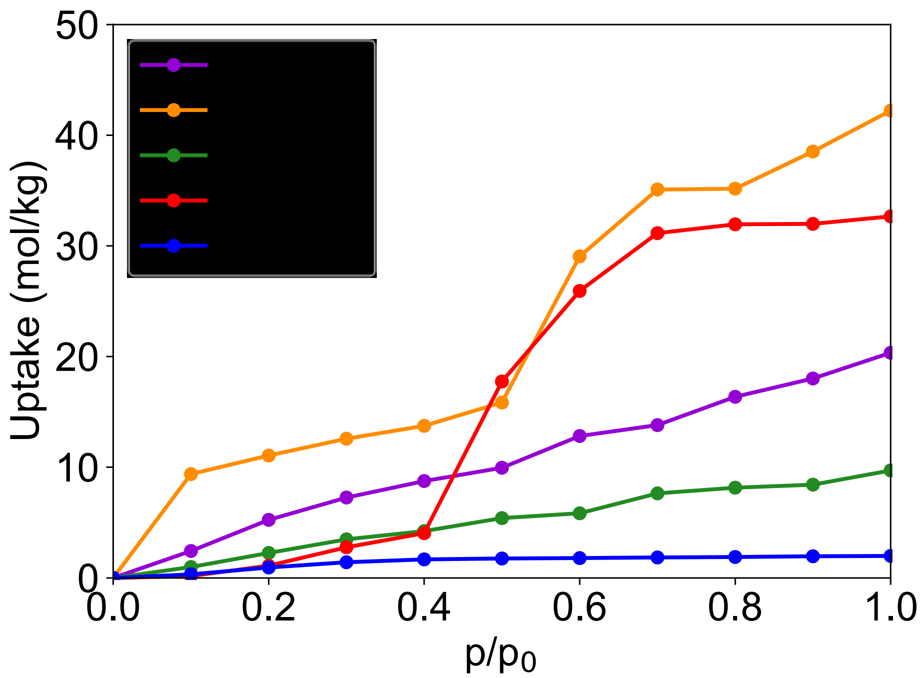

Figure S8. Ethanol adsorption isotherms of NU-1000, NU-100, NU-110, PCN-68 and PCN-777 at 303 K from GCMC simulations.

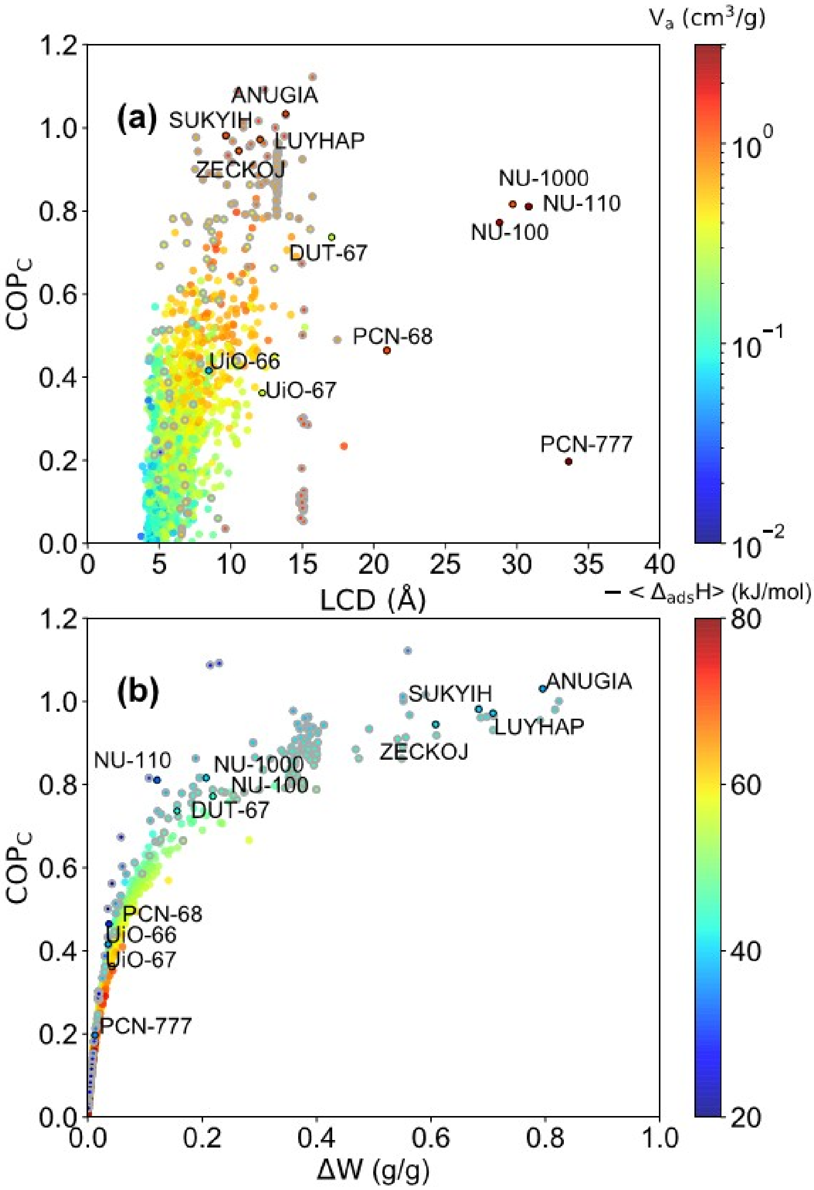

Figure S9. The correlation between (a) COP_C and LCD and (b) COP_C and ΔW, in which the MOFs with $0.1 < \alpha' < 0.2$ were highlight by gray circles.

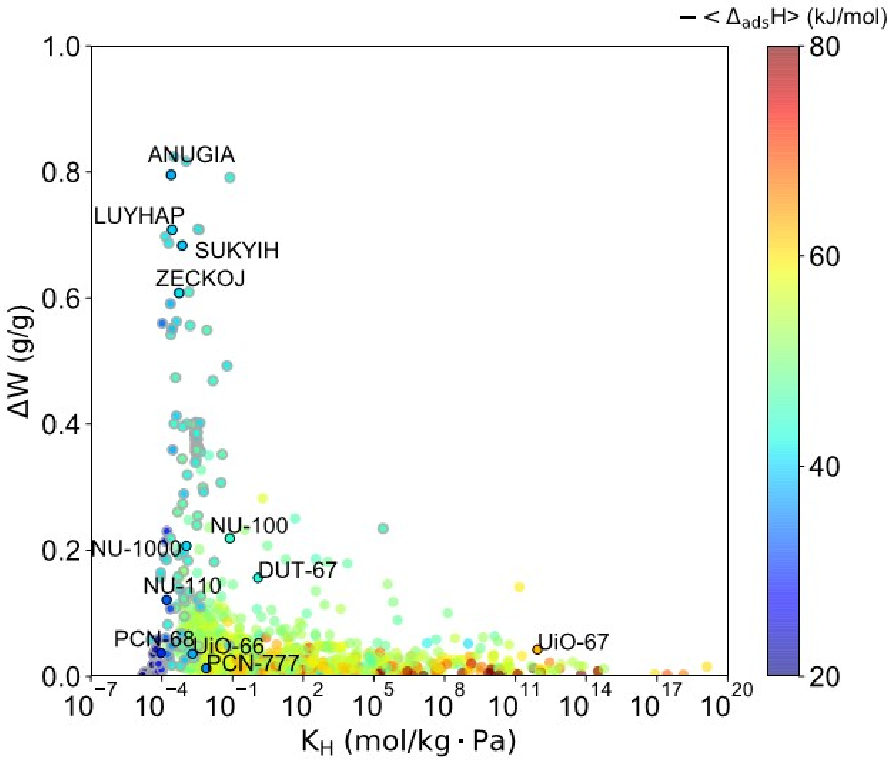

Figure S10. The correlation between Henry's constant and the working capacity of 1527 CoRE MOFs colored by average enthalpy of adsorption at T= 303 K. The MOFs with 0.1 < α' ≤ 0.2 were highlighted by gray circles.

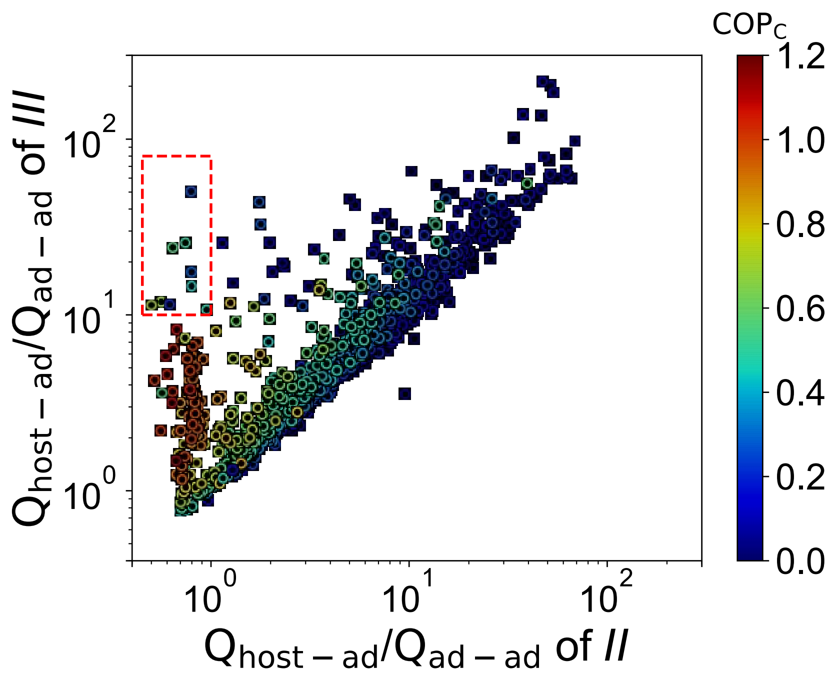

Figure S11. The correlation between the ratio of host-adsorbate interaction to adsorbate-adsorbate interaction ($Q_{host\text{-}ad}$ /$Q_{ad\text{-}ad}$) of preheating (*II* at 325 K) and desorption (*III* at 353 K) process. The structures within the dotted red box are the ones with $Q_{host\text{-}ad}/Q_{ad\text{-}ad}$ < 1 at preheating (*II*) and $Q_{host\text{-}ad}/Q_{ad\text{-}ad}$ > 10 at desorption (*III*).

Table S5. The structure property of the MOFs highlighted in Figure S10 with $Q_{host-ad}/Q_{ad-ad} < 1$ at preheating (*II*) and $Q_{host-ad}/Q_{ad-ad} > 10$ at desorption.

REFCODE	LCD (Å)	ASA (m^2/g)	V_a (cm^3/g)	W_{max} (g/g)	W_{min} (g/g)	Q_{total} of *II* (kJ/mol)	Q_{total} of *III* (kJ/mol)	COP_C
XOPVII	6.84	1325	0.35	0.25	0.23	-84.52	-84.53	0.24
GUYLOC	6.34	1431	0.38	0.25	0.22	-63.61	-63.33	0.29
XIDBUJ	7.47	1059	0.31	0.25	0.22	-60.23	-61.33	0.30
YARGAB	10.67	1352	0.49	0.33	0.28	-54.72	-56.07	0.43
FAKLIO	9.33	2094	0.69	0.43	0.39	-57.09	-57.34	0.46
HIHNUJ	7.99	2746	0.80	0.54	0.47	-49.34	-52.50	0.50
NINHOH	6.48	2413	0.65	0.31	0.23	-49.54	-52.52	0.56
VUSKEA	14.96	3684	1.26	0.06	0.01	-42.06	-47.21	0.67
ALULAV	8.90	5005	1.24	0.85	0.67	-48.92	-52.46	0.72

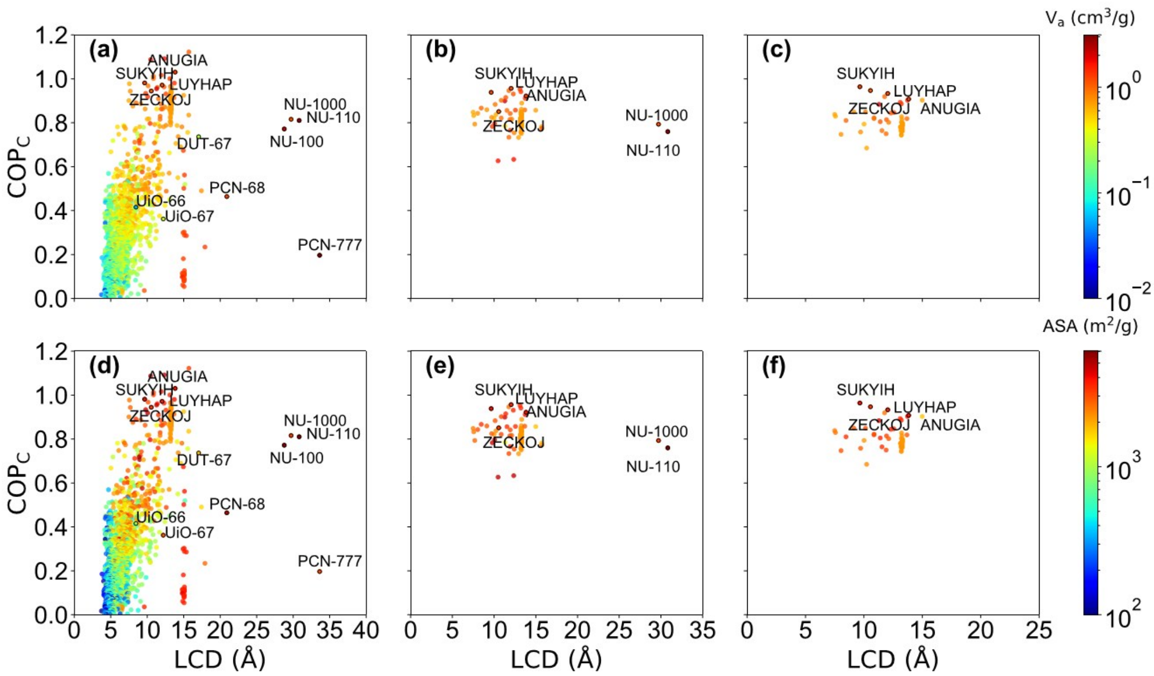

Figure S12. The structure-property relationship of the MOFs in each screening stage of the (a and d) first, (b and e) second and (c and f) third stage.

Table S6. Top 26 MOFs selected from the final stage of screening with $COP_C \geq 0.8$

No.	MOF Refcode	LCD (Å)	ASA (m^2/g)	V_a (cm^3/g)	COP_C	ΔW (g/g)	-<$\Delta_{ads}H$> (kJ/mol)
1	SUKYIH[2]	9.65	3884	1.20	0.96	0.90	42.35
2	ZECKOJ[3]	10.56	3190	1.06	0.95	0.63	42.08
3	LUYHAP[4]	12.04	3563	1.15	0.93	0.74	43.26
4	NIGBOW[5]	11.77	2528	0.97	0.92	0.57	43.12
5	ANUGIA[6]	13.83	3789	1.28	0.91	0.82	44.87
6	UTEWUM[7]	15.00	1766	0.70	0.90	0.40	42.23
7	MIL-88C[8]	13.74	3909	1.42	0.90	0.86	45.31
8	FEFDEB[9]	13.11	3488	1.31	0.89	0.84	45.75
9	FUNCEX[10]	13.22	3491	1.30	0.89	0.83	46.10
10	ECOLEP[11]	11.30	4555	2.07	0.88	1.00	46.71
11	XAMHEA[12]	9.14	2801	0.74	0.85	0.40	45.18
12	EGEJIK[13]	10.14	2930	0.89	0.85	0.58	47.02
13	FUNBOG[10]	12.57	3339	1.23	0.85	0.74	48.05
14	BICDAU[14]	12.31	3558	1.10	0.84	0.71	48.07
15	HIFVUO[15]	7.50	2392	0.65	0.84	0.30	43.87
16	MOXNUJ[16]	7.57	2434	0.66	0.83	0.36	45.87
17	DOTSOV35[17]	13.23	2138	0.71	0.83	0.36	45.92
18	YUGLES[18]	10.87	3069	0.96	0.82	0.56	48.55
19	NUTQAV[19]	10.87	3062	0.94	0.82	0.54	48.63
20	YURJUR[20]	13.69	2832	0.96	0.82	0.57	48.86
21	XADDIR[21]	13.26	2224	0.72	0.82	0.39	47.22
22	IYIHUU[22]	11.94	3059	1.03	0.81	0.56	49.11
23	TEDGOA[23]	8.47	3311	0.97	0.81	0.57	49.43
24	HIGRIA[14]	11.40	3509	1.09	0.80	0.70	50.51
25	XAMDUM[24]	13.22	2139	0.72	0.80	0.39	48.00
26	NUTQEZ[25]	12.12	2786	0.87	0.80	0.44	48.78

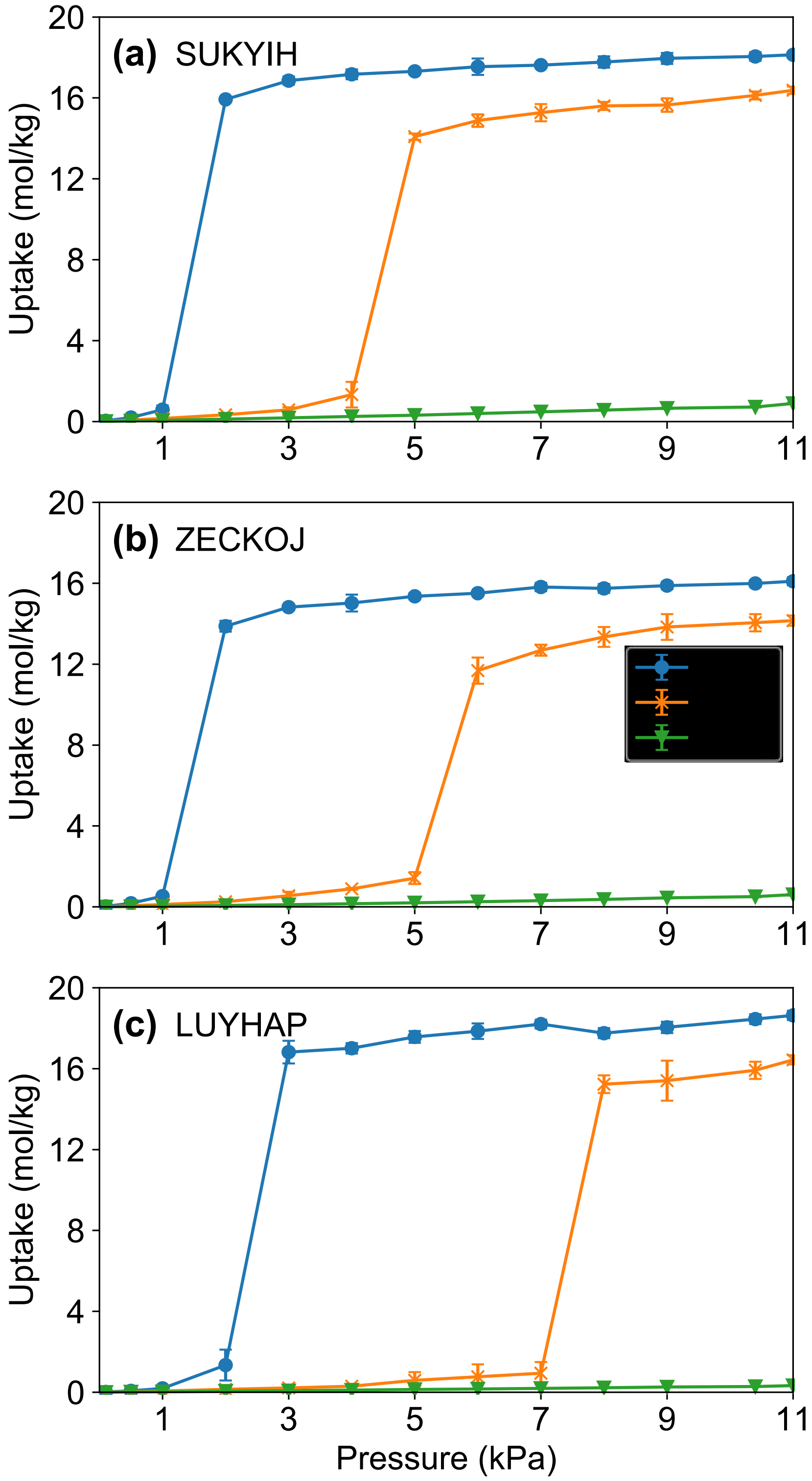

Figure S13. Ethanol adsorption isotherms of the selected top three MOFs: (a) SUKYIH, (b) ZECKOJ and (c) LUYHAP at 303 K, 325 K and 353 K.

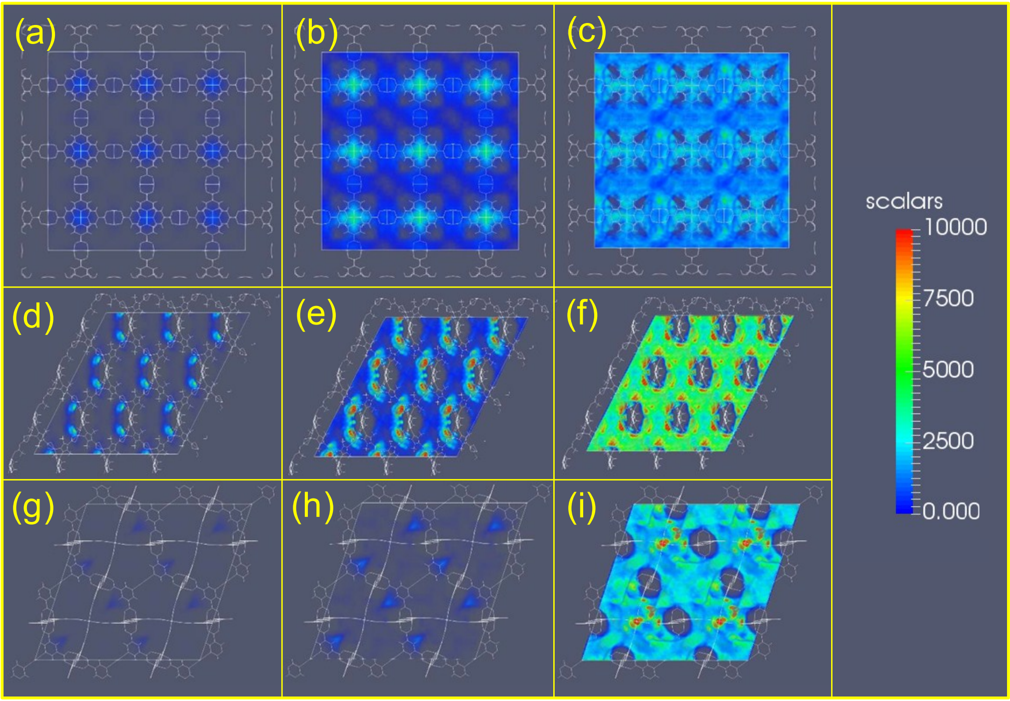

Figure S14. The density distribution maps of ethanol within the top three MOFs structures: (a) SUKYIH at 325 K and 1000 Pa; (b) SUKYIH at 325K and 4000 Pa; (c) SUKYIH at 325K and 10400 Pa; (d) ZECKOJ at 325 K and 1000 Pa; (e) ZECKOJ at 325 K and 4000 Pa; (f) ZECKOJ at 325 K and 10400 Pa; (g) LUYHAP at 325 K and 1000 Pa; (h) LUYHAP in 325 K, 4000 Pa; (i) LUYHAP in 325 K and 10400 Pa.

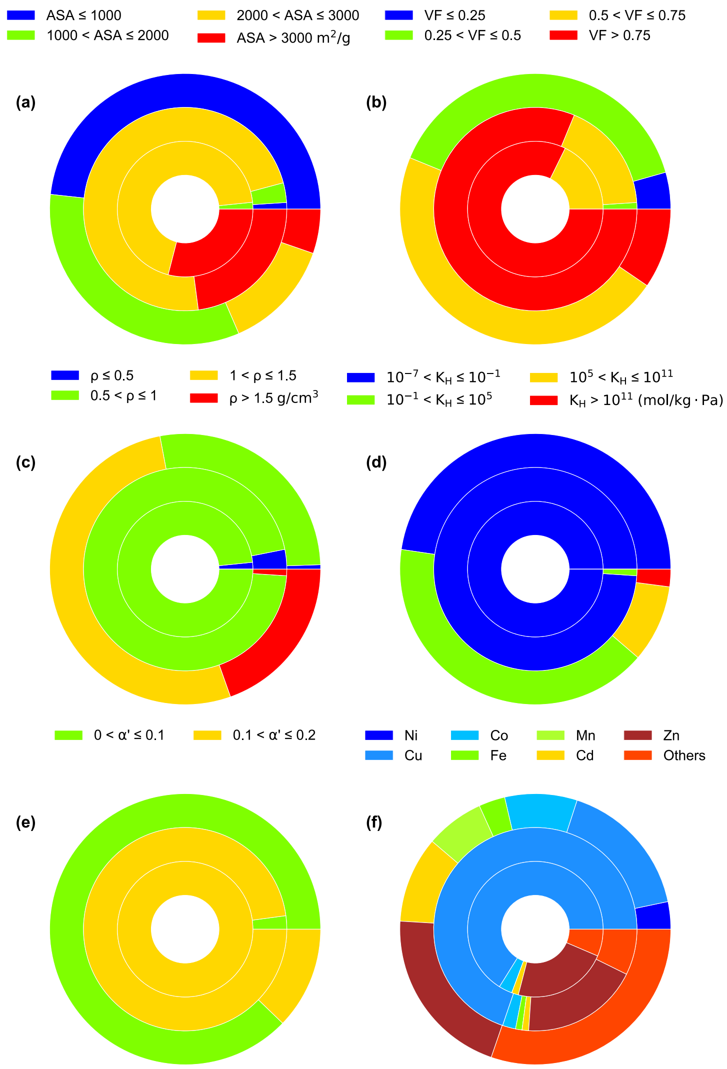

Figure S15. (a) Accessible surface area (ASA), (b) helium void fraction (VF),(c) density (ρ), (d) ethanol Henry's constant (K_H),(e) step position (α') and (f) metal types of CoRE MOFs in the first, second and third round of screening (from the outer to the inner). The number of CoRE MOFs in the first, second and third round of screening are 1527, 94 and 61, respectively.

Table S7. The average atomic partial charges for metal elements of 1527 CoRE MOFs

Metal type	q (e)	# of MOFs	Metal type	q (e)	# of MOFs	Metal Type	q (e)	# of MOFs
Re	-0.1	6	K	0.93	12	Al	1.84	14
Ir	-0.07	1	Pb	0.93	3	Lu	1.86	3
Au	-0.02	1	Co	0.94	133	Sb	1.99	1
Pt	0.02	4	Na	0.95	7	Sc	2.05	3
Se	0.04	2	Fe	0.95	49	Ti	2.05	1
Rh	0.04	1	Ru	1.07	8	Y	2.07	18
Te	0.14	1	Mn	1.1	110	Tm	2.14	10
Ag	0.3	24	Bi	1.14	2	La	2.15	42
Nb	0.4	1	Be	1.22	2	Pr	2.15	19
As	0.44	1	Sn	1.34	1	Ho	2.16	15
Pd	0.46	2	Si	1.38	14	Gd	2.17	39
Hg	0.46	3	Er	1.48	23	Ce	2.21	23
B	0.66	3	Yb	1.49	14	Np	2.23	1
Ni	0.7	71	Mg	1.55	25	Sm	2.25	21
Cu	0.71	261	Cr	1.56	6	Nd	2.27	40
Mo	0.82	12	Ga	1.57	5	U	2.27	12
Cd	0.88	161	Ca	1.58	13	Zr	2.28	5
Li	0.88	8	In	1.6	14	Dy	2.28	26
W	0.89	11	Sr	1.62	5	Hf	2.49	2
Zn	0.9	351	Ba	1.62	7			
Rb	0.92	2	V	1.75	21			

Note: among 1527 MOFs, 1365 MOFs only possess a single type of metal element, thus it was counted only once for the number of MOFs in Table S6; 156 MOFs possess two types of metals, which was counted twice. Similarly, 5 MOFs with three types of metals were counted three times and one MOF with four types of metals was counted four times.

S3. Details of COP_C calculation by mathematical model

S3.1 MOF Synthesis and Adsorption Measurements

Materials and synthesis: All chemicals required in this study were used as received (without any purification) from commercial sources. Zirconium chloride ($ZrCl_4$, 99.95%) from J&K China Chemical Ltd. Zirconyl chloride octahydrate ($ZrOCl_2 \cdot 8H_2O$, 99.9%), benzoic acid (99.9%) and 1,4-benzenedicarboxylic acid (H_2BDC, 99%) from Aladdin. Biphenyl-4,4'-dicarboxylic acid (H_2BPDC, 98%) and tetraethyl 4,4',4'',4'''-(pyrene-1,3,6,8-tetrayl) tetrabenzoic acid (H_4TBAPy, 98%) from Zhengzhou Alfachem Co.,Ltd. N,N-dimethylformamide (DMF), acetic acid, hydrochloric acid (HCl), ethanol and acetone from Sinopharm Chemical Reagent Co., Ltd. (Shanghai, China, AR). UiO-66, UiO-67 and NU-1000 were synthesized according to previously reported protocol,[26-28] respectively.

Ethanol adsorption isotherm: The ethanol adsorption isotherms were measured by Quantachrome Autosorb-iQ2 sorption analyzer using absolute ethanol. For each measurement, 50 mg of sample was used. Each sample was outgassed under vacuum at 353 K and 393 K for 0.5 and 24 h, respectively. After outgassing, the sample was measured at 293 K and 303 K, respectively. Ethanol vapor adsorption was measured at relative pressure (P/P_0) ranging from 0.001 to 1.0 P was the pressure of ethanol vapor in the sample cell when equilibrium has been achieved. P_0 was the saturation pressure of ethanol vapor at the working temperature.

S3.2 COP_C calculation by mathematic model

To predict the equilibrium uptake of ethanol of synthesized MOFs at varying temperatures, we used a universal isotherm model[29] (Eq. S14) to fit the experimentally measured isotherms of UiO-66, UiO-67 and NU-1000.

$$W = \sum_{i=1}^{n} \alpha_i \left\{ \frac{\left(\frac{p}{p_0} \exp\left(\frac{\varepsilon oi}{RT}\right) \right)^{\frac{RT}{m_i}}}{1 + \left(\frac{p}{p_0} \exp\left(\frac{\varepsilon oi}{RT}\right) \right)^{\frac{RT}{m_i}}} \right\}_i \quad \text{Eq. S14}$$

W is the adsorption uptake, P stands for the equilibrium pressure, P_o represents the saturation pressure of working fluids. α_i is an introduced probability factor to meaningfully capture the characteristics of the energy distribution of adsorption sites over the heterogeneous surface and the sum of all of the probability factors equals one, i.e., $\sum_{i=1}^{n} \alpha_i$. ε_{oi} represents the adsorption energy site with maximum frequency; m_i represents the surface heterogeneity or the range of the energy sites available for the adsorption. The value of *n*, which reflects the complexity in form of multi-layer behavior, is determined by the characteristics of adsorption isotherms. Here, the parameters of Eq. S14 were obtained by fitting of experimentally measured adsorption isotherms of ethanol for UiO-66, UiO-67 and NU-1000, which are provided in Table S8.

Table S8. Parameters used in the universal isotherm model of UiO-66, UiO-67 and NU-1000.

	n	α	ε_o	m_i
UiO-66	3	$\alpha_1=0.04544$	$\varepsilon_{o1}=5.96\times10^3$	$m_1=3.8\times10^2$
		$\alpha_2=0.24906$	$\varepsilon_{o2}=7.33\times10^3$	$m_2=3.37\times10^3$
		$\alpha_3=0.70550$	$\varepsilon_{o3}=2.01\times10^{-13}$	$m_3=5.50\times10^2$
UiO-67	3	$\alpha_1=0.29067$	$\varepsilon_{o1}=6.72\times10^3$	$m_1=1.78\times10^2$
		$\alpha_2=0.25129$	$\varepsilon_{o2}=5.98\times10^3$	$m_2=2.90\times10^3$
		$\alpha_3=0.45805$	$\varepsilon_{o3}=3.07\times10^{-9}$	$m_3=4.46\times10^2$
NU-1000	4	$\alpha_1=0.11182$	$\varepsilon_{o1}=3.20\times10^3$	$m_1=2.21\times10^2$
		$\alpha_2=0.39995$	$\varepsilon_{o2}=9.18\times10^2$	$m_2=4.84\times10^3$
		$\alpha_3=0.30481$	$\varepsilon_{o3}=2.78\times10^3$	$m_3=12.42$
		$\alpha_4=0.18342$	$\varepsilon_{o4}=7.27\times10^3$	$m_4=1.05\times10^3$

After obtaining the fitted isotherms at operation temperatures (Figure S16), the coefficient of performance for cooling (COP_C) can be calculated according to Eq. 1 based on the thermodynamic cycle diagram of adsorption cooling as shown in Figure 1. Clausius-Clapeyron equation was employed to obtain the enthalpy of adsorption by using the experimental isotherms of ethanol at different temperatures. The operation temperature was exactly the same as in computational screening base on GCMC simulations shown in Table S3. Finally, the calculated values of COP_C at given working condition were provided in Figure S17 and Table S9.

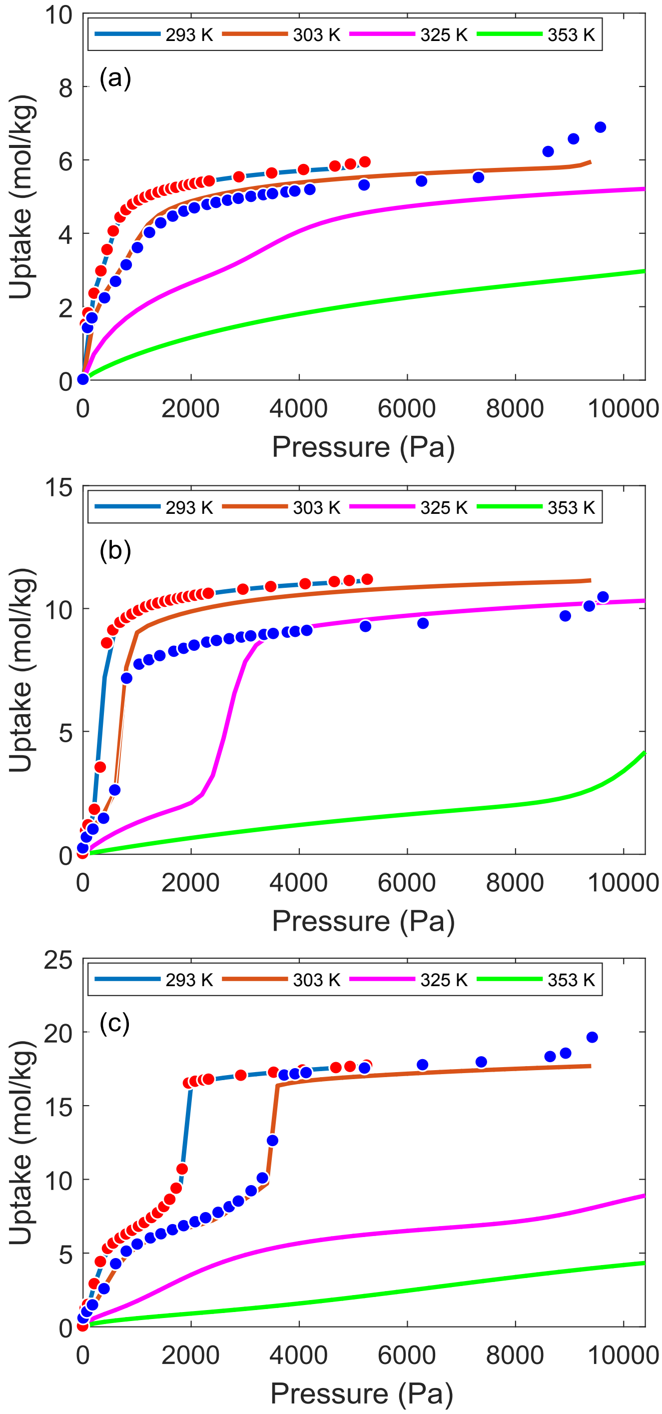

Figure S16. Fitted adsorption isotherms of ethanol of (a) UiO-66, (b) UiO-67, (c) NU-1000 by universal isotherm model. The red and blue dots represent experimental measured data, and the lines represent fitted data.

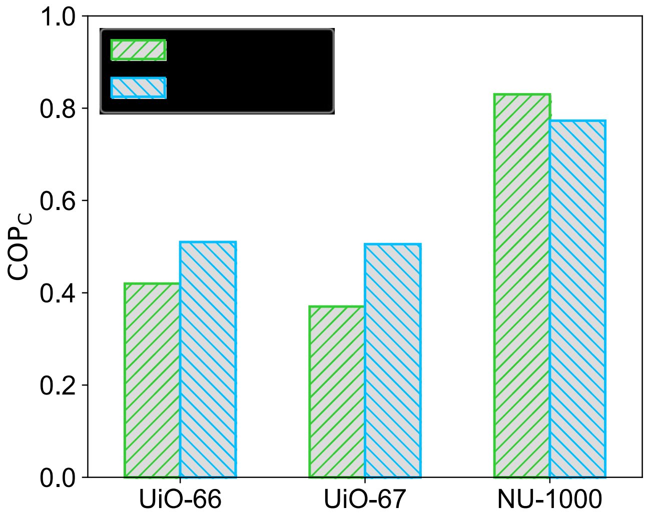

Figure S17. Comparison of COP_C for UiO-66, UiO-67 and NU-1000 by high-throughput computational screening based on GCMC simulations and those obtained from mathematic model based on experimentally measured ethanol adsorption isotherms at operating temperatures.

Table S9. COP_C of UiO-66, UiO-67 and NU-1000 from mathematical model and simulations

	UiO-66	UiO-67	NU-1000
COP_C from mathematical model	0.510	0.506	0.773
COP_C from GCMC simulation	0.416	0.362	0.816

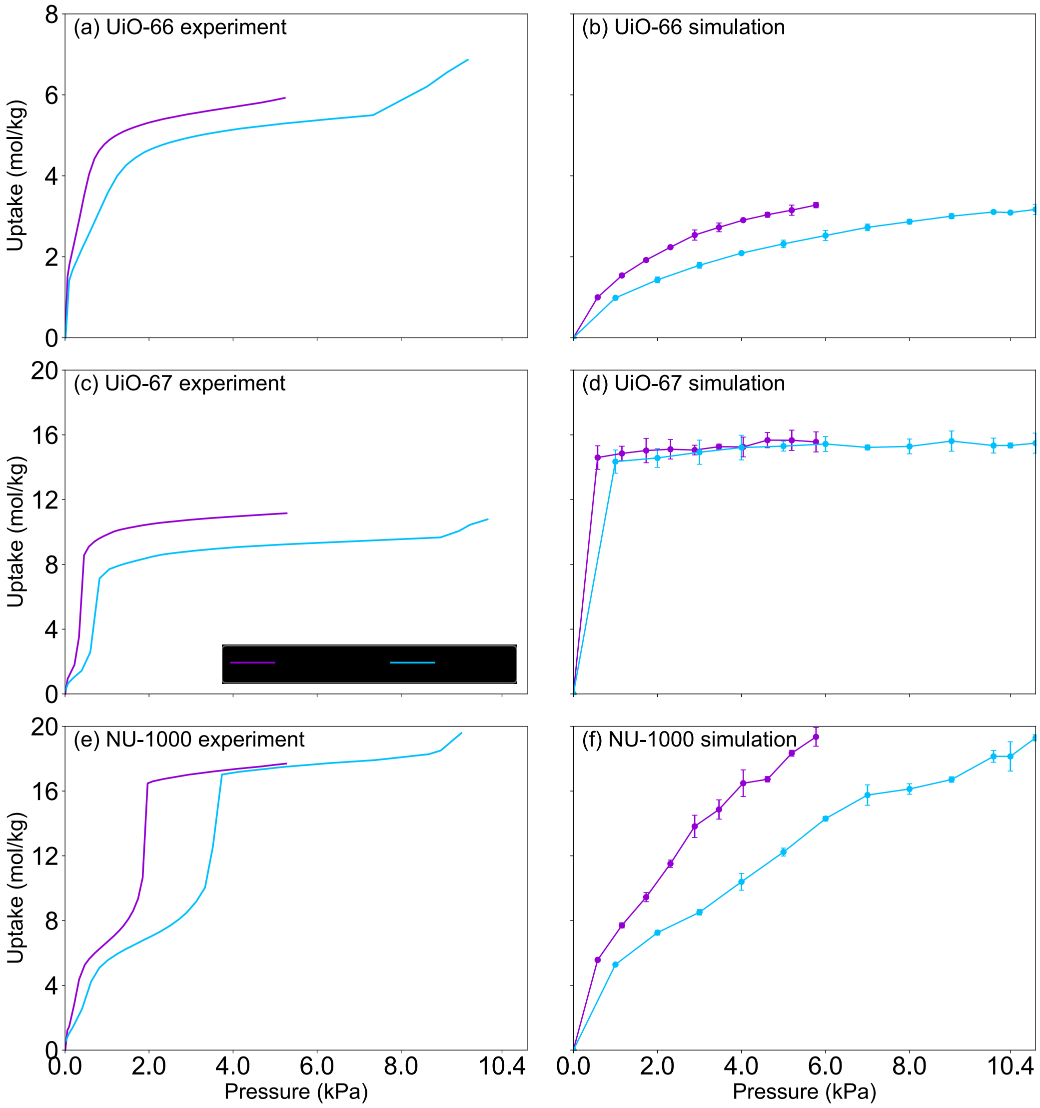

Figure S18. Ethanol adsorption isotherms of UiO-66, UiO-67 and NU-1000 obtained from experimental measurements in this work (a, c, e) and GCMC simulations (b, d, f) at 293 K and 303 K.

References

1. M. F. de Lange, K. J. F. M. Verouden, T. J. H. Vlugt, J. Gascon and F. Kapteijn, *Chem. Rev.*, 2015, **115**, 12205-12250.
2. L. Ma, A. Jin, Z. Xie and W. Lin, *Angew. Chem. Int. Ed.*, 2009, **48**, 9905-9908.
3. E. Quartapelle Procopio, T. Fukushima, E. Barea, J. A. Navarro, S. Horike and S. Kitagawa, *Chem. Eur. J.*, 2012, **18**, 13117-13125.
4. D. Zhao, D. Yuan, A. Yakovenko and H. C. Zhou, *Chem. Commun.*, 2010, **46**, 4196-4198.
5. Y. Y. Liu, S. Couck, M. Vandichel, M. Grzywa, K. Leus, S. Biswas, D. Volkmer, J. Gascon, F. Kapteijn, J. F. Denayer, M. Waroquier, V. Van Speybroeck and P. Van Der Voort, *Inorg. Chem.*, 2013, **52**, 113-120.
6. J. K. Schnobrich, O. Lebel, K. A. Cychosz, A. Dailly, A. G. Wong-Foy and A. J. Matzger, *J. Am. Chem. Soc.*, 2010, **132**, 13941-13948.
7. V. Colombo, S. Galli, H. J. Choi, G. D. Han, A. Maspero, G. Palmisano, N. Masciocchi and J. R. Long, *Chem. Sci.*, 2011, **2**, 1311-1319.
8. S. Surble, C. Serre, C. Mellot-Draznieks, F. Millange and G. Ferey, *Chem. Commun.*, 2006, **3**, 284-286.
9. P. V. Dau, M. Kim, S. J. Garibay, F. H. Munch, C. E. Moore and S. M. Cohen, *Inorg. Chem.*, 2012, **51**, 5671-5676.
10. O. K. Farha, C. D. Malliakas, M. G. Kanatzidis and J. T. Hupp, *J. Am.Chem. Soc.*, 2010, **132**, 950-952.
11. M. Li, D. Du, G. Yang, S. Li, Y. Lan, K. Shao, J. Qin and Z. Su, *Cryst. Growth & Des.*, 2011, **11**, 2510-2514.
12. R. K. Deshpande, G. I. Waterhouse, G. B. Jameson and S. G. Telfer, *Chem. Commun.*, 2012, **48**, 1574-1576.
13. A. D. Burrows, C. G. Frost, M. F. Mahon and C. Richardson, *Angew. Chem.Int. Ed.*, 2008, **47**, 8482-8486.
14. P. Schmieder, D. Denysenko, M. Grzywa, B. Baumgartner, I. Senkovska, S. Kaskel, G. Sastre, L. van Wullen and D. Volkmer, *Dalton Trans.*, 2013, **42**, 10786-10797.
15. Y. Q. Tian, Y. M. Zhao, Z. X. Chen, G. N. Zhang, L. H. Weng and D. Y. Zhao, *Chem. Eur. J.*, 2007, **13**, 4146-4154.
16. P. E. Ryan, C. Lescop, D. Laliberte, T. Hamilton, T. Maris and J. D. Wuest, *Inorg. Chem.*, 2009, **48**, 2793-2807.
17. Y. Wu, A. Kobayashi, G. J. Halder, V. K. Peterson, K. W. Chapman, N. Lock, P. D. Southon and C. J. Kepert, *Angew. Chem. Int. Ed.*, 2008, **47**, 8929-8932.
18. Y. Hu, S. Xiang, W. Zhang, Z. Zhang, L. Wang, J. Bai and B. Chen, *Chem. Commun.*, 2009, **48**, 7551-7553.
19. D. Sun, S. Ma, J. M. Simmons, J.-R. Li, D. Yuan and H.-C. Zhou, *Chem. Commun.*, 2010, **46**, 1329-1331.
20. E. Neofotistou, C. D. Malliakas and P. N. Trikalitis, *CrystEngComm*, 2010, **12**, 1034-1037.
21. F. Ma, S. Liu, D. Liang, G. Ren, C. Zhang, F. Wei and Z. Su, *Eur. J. Inorg.*

Chem., 2010, **2010**, 3756-3761.
22. C. Y. Lee, Y. S. Bae, N. C. Jeong, O. K. Farha, A. A. Sarjeant, C. L. Stern, P. Nickias, R. Q. Snurr, J. T. Hupp and S. T. Nguyen, *J. Am. Chem. Soc.*, 2011, **133**, 5228-5231.
23. G.-S. Yang, M.-N. Li, S.-L. Li, Y.-Q. Lan, W.-W. He, X.-L. Wang, J.-S. Qin and Z.-M. Su, *J. Mater. Chem.*, 2012, **22**, 17947-17953.
24. A. J. Graham, J. C. Tan, D. R. Allan and S. A. Moggach, *Chem. Commun.*, 2012, **48**, 1535-1537.
25. D. Sun, S. Ma, J. M. Simmons, J. R. Li, D. Yuan and H. C. Zhou, *Chem. Commun.*, 2010, **46**, 1329-1331.
26. A. Schaate, P. Roy, A. Godt, J. Lippke, F. Waltz, M. Wiebcke and P. Behrens, *Chem. Eur. J.*, 2011, **17**, 6643-6651.
27. S. Oien-Odegaard, B. Bouchevreau, K. Hylland, L. P. Wu, R. Blom, C. Grande, U. Olsbye, M. Tilset and K. P. Lillerud, *Inorg. Chem.*, 2016, **55**, 1986-1991.
28. T. C. Wang, N. A. Vermeulen, I. S. Kim, A. B. F. Martinson, J. F. Stoddart, J. T. Hupp and O. K. Farha, *Nat. Protoc.*, 2016, **11**, 149-162.
29. K. C. Ng, M. Burhan, M. W. Shahzad and A. B. Ismail, *Sci. Rep.*, 2017, **7**, 10634.